The EMBO Journal Vol. 22 No. 9 pp. 1969–1980, 2003

VirB11 ATPases are dynamic hexameric assemblies: new insights into bacterial type IV secretion

Savvas N.Savvides[1,2], Hye-Jeong Yeo[1,3], Moriah R.Beck[1], Franca Blaesing[4], Rudi Lurz[4], Erich Lanka[4], Renate Buhrdorf[5], Wolfgang Fischer[5], Rainer Haas[5] and Gabriel Waksman[1,3,6,7]

[1]Department of Biochemistry and Molecular Biophysics, Washington University School of Medicine, 660 S. Euclid Ave, St Louis, MO 63110, USA, [3]School of Crystallography, Birkbeck College, Malet Street, London WC1E 7HX, [6]Department of Biochemistry and Molecular Biology, University College London, Gower Street London, WC1E 6BT, UK, [4]Max Planck Institut für Molekulare Genetik, Ihnestrasse 73, Dahlem, D-14195 Berlin and [5]Max von Pettenkofer Institut, LMU Munich, Pettenkoferstrasse 9a, D-80336 Munich, Germany

[2]Present address: Department of Ultrastructure, Vlaams Interuniversitair Instituut voor Biotechnologie, Vrije Universiteit Brussel, Pleinlaan 2, 1050 Brussels, Belgium

[7]Corresponding author
e-mail: g.waksman@mail.cryst.bbk.ac.uk

S.N.Savvides and H.-J.Yeo contributed equally to this work

The coupling of ATP binding/hydrolysis to macromolecular secretion systems is crucial to the pathogenicity of Gram-negative bacteria. We reported previously the structure of the ADP-bound form of the hexameric traffic VirB11 ATPase of the *Helicobacter pylori* type IV secretion system (named HP0525), and proposed that it functions as a gating molecule at the inner membrane, cycling through closed and open forms regulated by ATP binding/hydrolysis. Here, we combine crystal structures with analytical ultracentrifugation experiments to show that VirB11 ATPases indeed function as dynamic hexameric assemblies. In the absence of nucleotide, the N-terminal domains exhibit a collection of rigid-body conformations. Nucleotide binding 'locks' the hexamer into a symmetric and compact structure. We propose that VirB11s use the mechanical leverage generated by such nucleotide-dependent conformational changes to facilitate the export of substrates or the assembly of the type IV secretion apparatus. Biochemical characterization of mutant forms of HP0525 coupled with electron microscopy and *in vivo* assays support such hypothesis, and establish the relevance of VirB11s ATPases as drug targets against pathogenic bacteria.

Keywords: bacterial pathogenesis/crystal structure/*Helicobacter pylori*/HP0525/VirB11 ATPases

Introduction

Virulence and pathogenesis in Gram-negative bacteria rely in part on macromolecular secretion machineries (types I–V) that specialize in the task of translocating proteins and/or protein–DNA complexes from the bacterial cytosol to the host cell through the bacterial double-membrane system (Thanassi and Hultgren, 2000). These secretion systems are multi-protein assemblies constructed from both soluble and membrane-associated proteins, and employ essential NTPases (predominantly ATPases) that energize the assembly of these secretion systems and/or substrate translocation.

One such family of NTPases is that of the PulE-like proteins that are part of type II and type IV secretion machineries (Possot and Pugsley, 1994; Christie and Vogel, 2000) found in a variety of important human pathogens such as enteropathogenic *Escherichia coli* causing infant diarrhoea (type II secretion), *Pseudomonas aeruginosa*, a leading cause of opportunistic infections in immunocompromised patients (type II secretion), *Helicobacter pylori*, which causes peptic ulcer diseases (type IV), and *Legionella pneumophila*, which causes pneumonia (type IV secretion) (Finlay and Falkow, 1997; Vogel *et al*., 1998). While the absolute requirement of these NTPases for proper functioning of their respective secretion machineries is well established (Christie and Vogel, 2000), several important questions regarding their specific role and mode of action remain unanswered. In fact, their role may vary from one organism to another depending on the type of transport they help to mediate.

Type IV secretion systems require a subclass of PulE-like NTPases collectively known as VirB11 ATPases (Christie and Vogel, 2000). Recent studies on three VirB11 NTPases, TrbB and TrwD from the RP4 and R388 plasmid conjugative systems, and HP0525 from the type IV secretion system of *H.pylori*, have provided a consensus of their general biochemical properties (Rashkova *et al*., 1997; Krause *et al*., 2000a,b; Machón *et al*., 2002) suggesting an underlying common mode of action among VirB11 NTPases. Although their nucleotide requirements vary, NTPase activity is enhanced by lipid binding, consistent with the localization and/or partial association of VirB11 NTPases to the bacterial inner membrane. Structurally, these proteins form hexameric ring assemblies, reminiscent of nucleotide-dependent molecular motors such as helicases and F1-ATPases (Krause *et al*., 2000a; Yeo *et al*., 2000; Machón *et al*., 2002), and membrane fusion proteins such as NSF and p97 (Lenzen *et al*., 1998; Zhang *et al*., 2000). A fundamental but thus far unanswered question has been how such ring complexes harness the energy from nucleotide binding/hydrolysis to elicit conformational changes necessary for their respective cellular functions.

To elucidate the molecular features and structural determinants that dictate the activity and mode of action of VirB11 ATPases, we initiated a series of structural studies on HP0525 of the *H.pylori* type IV secretion

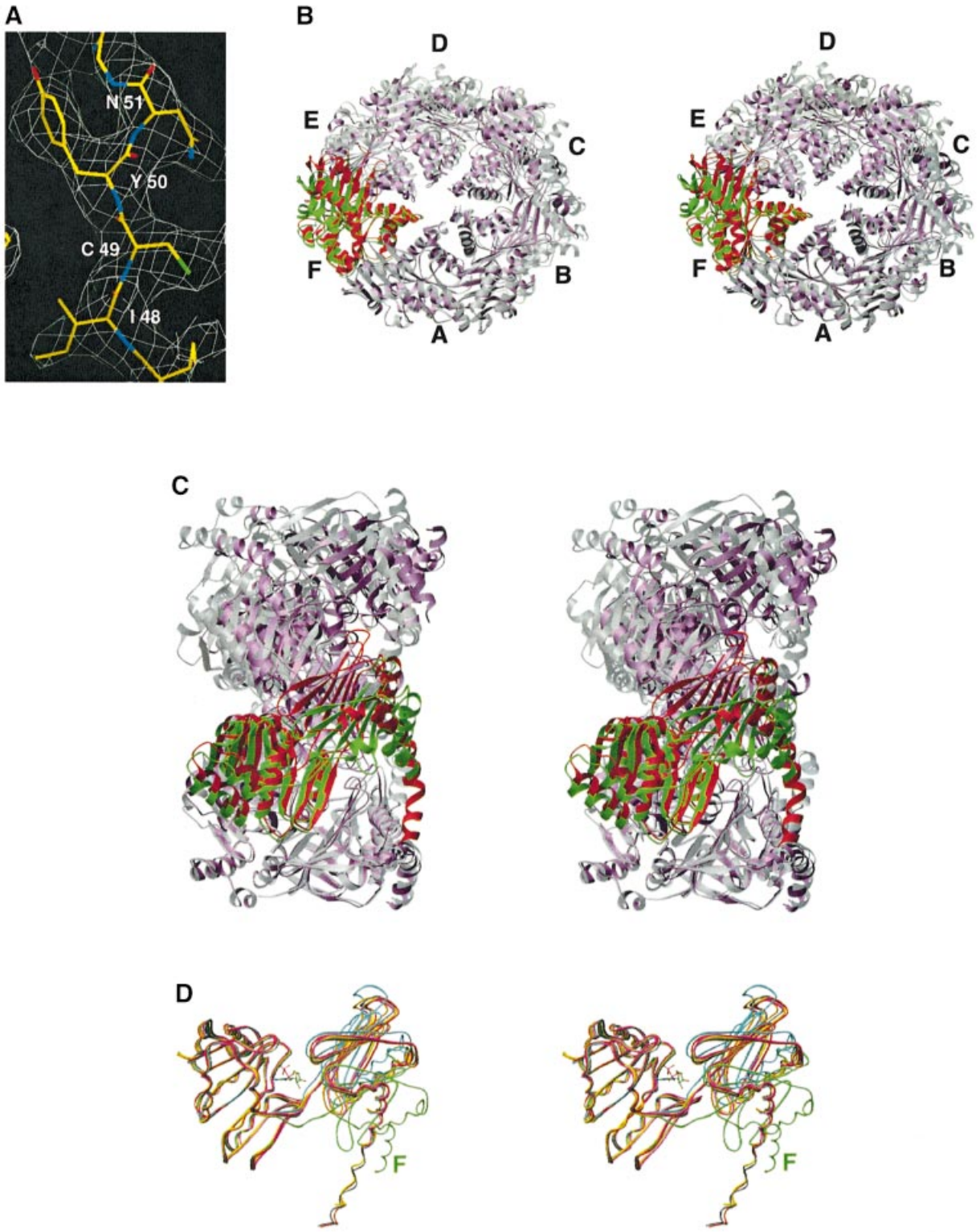

Fig. 1. Structure of apo-HP0525. (**A**) Representative region (the β1 strand of molecule A) of the experimental solvent-flattened electron density map at 3.0 Å resolution (contoured at 1.5σ) overlaid with the final refined model (Jones *et al*., 1991). (**B**) Stereo diagram of the structural superposition of apo-HP0525 (violet) and the ADP–HP0525 complex (gray) (Carson, 1997). The notation A–F is arbitrary, with molecule A defined as the first subunit listed in the PDB coordinate files of the unbound and ATPγS-bound structures. The two hexameric assemblies were overlaid with respect to molecule A of ADP–HP0525. Molecule F exhibits the largest conformational change and is colored green (apo-HP0525) and red (ADP–HP0525) in apo-HP0525 and ADP–HP0525, respectively. (**C**) Side view of the hexameric assemblies. This orientation is obtained by rotating the molecules shown in (B) 90° anti-clockwise along the vertical axis of (B). This view documents the extent of the conformational change in subunit F. (**D**) Structural variability between individual subunits in apo-HP0525. The overlay was carried out with respect to the CTD of subunit A of ADP–HP0525 (red). Subunit F of apo-HP0525 (green) exhibits the largest rotation (~15° more open) about the hinge region between the NTD and CTD. The coloring scheme for all other subunits is as follows: apo-HP0525_A, dark gray; apo-HP0525_B, pink; apo-HP0525_C, orange; apo-HP0525_D, yellow; apo-HP0525_E, cyan.

system. *H.pylori* is the causative agent of peptic ulcers, MALT-lymphoma and adenocarcinoma of the stomach, and constitutes one of the most common chronic infections in humans by colonizing the gastric epithelium (Wotherspoon, 1998; Graham, 2000). The infection process is associated with the translocation of a bacterial protein, CagA, to the host cell, which once injected becomes phosphorylated and is thought to interfere with signaling in the host cell (Segal *et al*., 1999; Asahi *et al*., 2000; Backert *et al*., 2000; Odenbreit *et al*., 2000; Stein *et al*., 2000). In a previous study, we reported the crystal structure of hexameric HP0525 in a complex with ADP (ADP–HP0525), which emerged as a structural prototype for VirB11 NTPases (Yeo *et al*., 2000). ADP–HP0525 assembles as a 'six-clawed grapple' possibly facing the cytosol and formed by the C-terminal domains (CTDs) of HP0525. This grapple is mounted onto a hexameric ring consisting of the N-terminal domains (NTDs) of the protein. Overall, ADP–HP0525 forms a dome-like internal chamber closed at one end and open at the other. The NTDs and CTDs sandwich the bound nucleotide and stack as separate rings around the hexameric assembly, with the NTDs defining the open side (internal diameter of 50 Å) and the CTDs contributing the 'six-clawed grapple' at the closed end (internal diameter of 10 Å). Based on the molecular features of ADP–HP0525, we suggested that HP0525 serves as a traffic ATPase at the bacterial inner membrane responsible for the translocation of CagA protein and/or components of the type IV secretion machinery. We further proposed that HP0525 carries out this function by cycling through closed and open forms that are regulated by ATP binding/hydrolysis and ADP release, respectively (Yeo *et al*., 2000).

Here, we derive new insights into the function and mode of action of VirB11 ATPases from molecular snapshots of the nucleotide-free form of HP0525 (apo-HP0525) and of the ATPγS-bound form (ATPγS–HP0525) complemented by sedimentation velocity, electron microscopy, mutagenesis and *in vivo* assay experiments. We provide direct evidence that VirB11 ATPases may function as dynamic hexameric assemblies, which upon nucleotide binding (not hydrolysis) undergo rigid-body swiveling of their NTDs to convert open and asymmetric hexamers to compact and symmetrically hexameric structures. The ensuing mechanical force generated from this 'locking' event could potentially be used to facilitate the assembly/disassembly of macromolecular complexes relevant to the export of substrates and/or the assembly of the type IV secretion apparatus itself.

Results and discussion

Structure of apo-HP0525

The apo structure was obtained using form B crystals (sulfate-free crystallization conditions) as described in Materials and methods. The structure of apo-HP0525 at 3.0 Å resolution reveals an asymmetric hexameric assembly that is significantly different from our previously determined structure of the ADP–HP0525 complex (Figure 1; Table I). While the CTD ring retains its previously observed 'six-clawed grapple' that forms the apex of the dome-like internal chamber, the NTDs exhibit

Table I. Data collection[a], phasing and refinement

Data collection	Resolution (Å)	Reflections (total/unique)	Completeness (%)	R_{sym} (%)[b]	$I/\sigma(I)$
Data set					
apo-HP0525					
SeMet-1, 0.9793 Å	30–3.0	290380/73729	89.5 (88.6)	8.5 (36.5)	14.9 (4.8)
SeMet-1, 0.9793 Å, Friedel pairs merged	30–3.0	288832/37255	90.5 (89.8)	10.7 (37.1)	18.0 (5.9)
SeMet-2, 0.9794 Å	30–3.0	291962/74172	89.4 (88.7)	8.3 (38.2)	15.2 (4.5)
SeMet-3, 0.9667 Å	30–3.0	290890/74148	89.2 (88.7)	8.1 (42.5)	15.6 (4.4)
ATPγS–HP0525					
SeMet-1, 0.9793 Å, Friedel pairs merged	30–2.8	110109 /21297	99.1 (99.7)	9.5 (37.8)	15.0 (4.1)
HP0525–sulfate					
SeMet-1, 0.9793 Å, Friedel pairs merged	30–2.8	80168/18699	87.0 (94.0)	11.5 (15.6)	10.4 (8.1)

Refinement	apo-HP0525	ATPγS–HP0525	HP0525–sulfate
Resolution (Å)	30–3.0	30–2.8	30–2.8
$\|F\|/\sigma(\|F\|)$	>0	>2	>2
Number of reflections (working/test)	34776/1821	15360/773	15592/728
Total number of atoms	14515	5245	5130
Protein molecules	6	2	2
ATPγS		2	
Mg^{2+}		1	
SO_4^{2-}		1	2
PEG (n = 9)		1	1
Water molecules	21	41	23
R_{cryst}, R_{free}	0.239, 0.298	0.243, 0.304	0.250, 0.324
R.m.s.ds			
Bonds (Å)	0.013	0.012	0.010
Angles (°)	1.53	1.43	1.36
B values (Å^2) (main chain/side chain)	1.8/2.5	1.8/2.7	1.5/2.3

[a]Numbers in parentheses correspond to values in the highest resolution shell [3.1–3.0 (apo-HP0525); 2.9–2.8 (ATPγS–HP0525 and HP0525–sulfate)].
[b]$R_{sym} = \Sigma|I - \langle I\rangle|/\Sigma I$, where I = observed intensity, and $\langle I\rangle$ = average intensity for symmetry-related reflections.

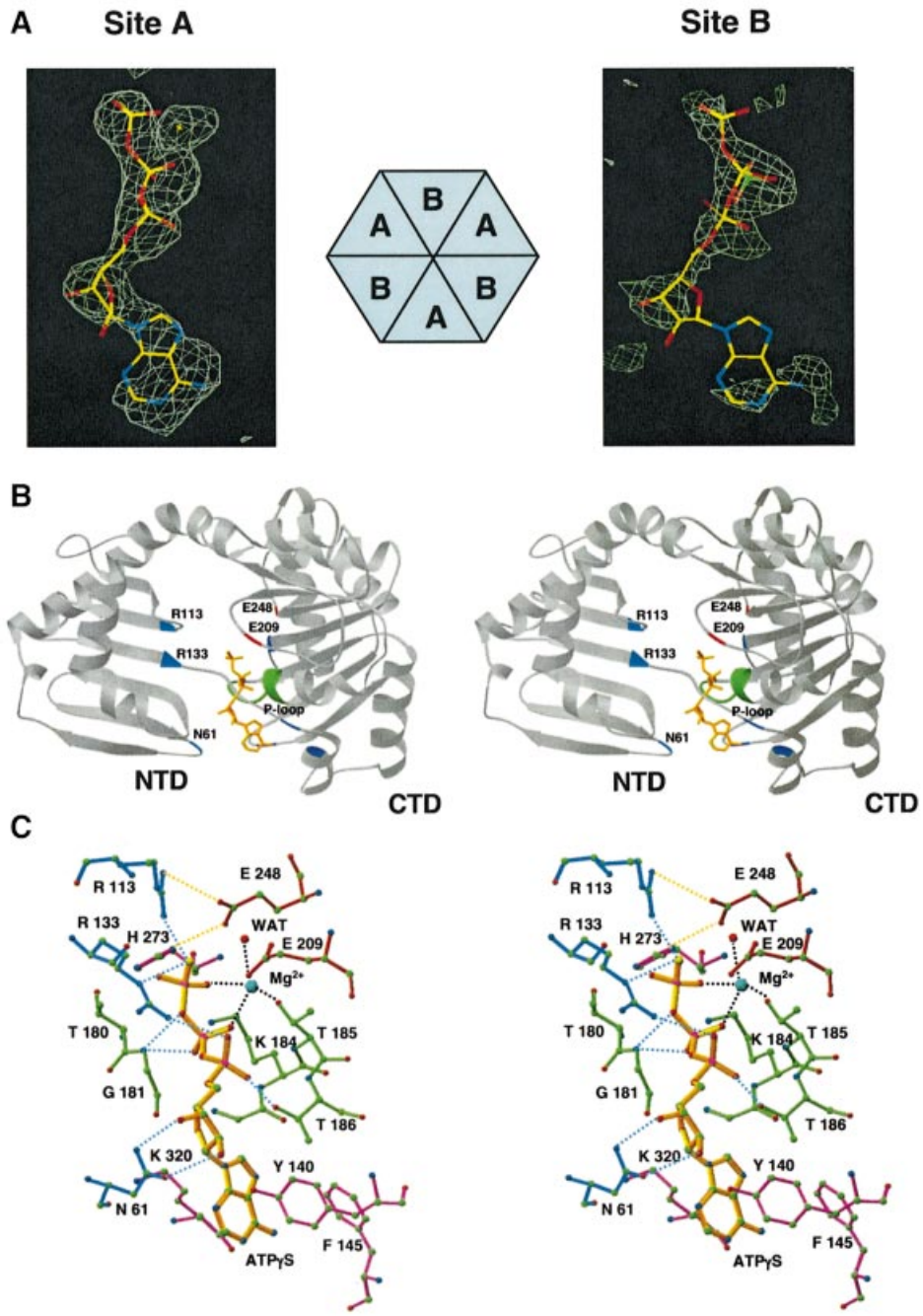

Fig. 2. Structure of the ATPγS–HP0525 complex. (**A**) Simulated annealing omit F_o–F_c electron density maps contoured at 3σ, illustrating the relative binding of ATPγS in molecules A and B of the ATPγS–HP0525 complex (Jones *et al*., 1991). The β-phosphate position of ATPγS in site B is co-occupied by a sulfate ion. (**B**) Stereo diagram of subunit A of the ATPγS–HP0525 complex with the various components of the ATPγS binding site mapped onto the tertiary structure (Carson, 1997). ATPγS is colored in gold, while regions of the subunit interacting with the nucleotide are shown as follows: NTD residues (blue), P-loop (green), the putative catalytic Glu248 and Glu209 (red), CTD residues other than Glu248, Glu209 and P-loop residues (purple). (**C**) Stereo diagram of the ATPγS binding site in molecule A (site A) of the ATPγS–HP0525 complex. Coordination of a magnesium ion by ATPγS, the protein and a water molecule is shown in black dashed lines. Hydrogen bonds between HP0525 and ATPγS are shown in cyan dashed lines, while orange dashed lines illustrate the bifurcated hydrogen bonding interactions of Arg113 and His273 with the proposed catalytic Glu248 (see main text). For consistency, this view and the color coding of bonds are the same as in (B).

rigid-body rotations about the linker region between the NTD and CTD (residues 134–141) and away (i.e. outward) from the center of the chamber (Yeo *et al*., 2000) (Figure 1B–D). The motion does not affect all subunits equally. The NTD of subunit A (see Figure 1B for notation of subunits) rotates by 2°, while the NTD of subunit F undergoes a 15° rotation. The extent of the rotation of the NTDs in all other subunits is between these two extremes (see Figure 1D). Electron density for the entire N-terminal αA helix of subunits B, C, E and F was missing, and only parts of this helix could be built in subunits A and D. The αA helix participates in subunit–subunit interactions and forms an extended arm that surrounds the NTD of the adjacent subunit in the hexamer (Yeo *et al*., 2000). While

the αA helix is not part of the nucleotide-binding site, it contains charged residues that make ionic and hydrogen bonding interactions with amino acids adjacent to the nucleotide-binding site (Yeo *et al*., 2000). Thus, nucleotide release may induce long-range effects that lead to the destabilization of the αA helix and consequently of the entire NTD.

Although the observed structural rearrangements in the NTDs vary in amplitude, we observe that subunits that are directly across from each other display similar behavior, which may have mechanistic relevance. For instance, subunits A and D are essentially identical [root mean squared deviation (r.m.s.d.) of 0.6 Å for 312 Cα atoms] and also match closely their counterparts in the ADP–HP0525 (ADP–HP0525_A versus apo-HP0525_A, r.m.s.d, 0.9 Å for 323 Cα atoms; ADP–HP0525_A versus apo-HP0525_D, r.m.s.d., 0.6 Å for 319 Cα atoms). A second example is that opposing subunits C and F exhibit the most dramatic deviations from ADP–HP0525, with the NTD of subunit C being the most disordered (only residues 28–76 and 101–330 were observed, $B_{main\ chain}$ = 70 Å^2), while the NTD of subunit F is the most displaced (Figure 1D). Calculation of the buried surface areas in subunit–subunit interfaces shows a similar trend, with 2280 and 2190 Å^2 at the A–B and opposite D–E interfaces, respectively, 1900 and 1840 Å^2 at the B–C and opposite E–F interfaces, respectively, 2000 and 2020 Å^2 at the C–D and opposite F–A interfaces, respectively.

The asymmetry and structural variability among the NTDs in apo-HP0525 support our previous prediction that in the absence of nucleotide, there is little to hold the CTDs and NTDs together, leading to destabilization of either the CTD or NTD ring in the hexamer (Yeo *et al*., 2000). More importantly, however, the structure of apo-HP0525 provides evidence that VirB11s are indeed dynamic molecular assemblies and that they may use such a feature to carry out their respective functions. We can now also define more precisely the role of each of the two domain rings. Since the CTD ring remains unchanged, a likely role for the CTDs is to drive oligomerization. In contrast, the NTD ring undergoes large deformation and can rearrange according to the required function (see below).

Structure of the ATPγS–HP0525 complex

To obtain a representative picture of the nucleotide-binding environment that most closely resembles that of the physiological substrate ATP, we sought to determine the structure of HP0525 bound to the non-hydrolysable ATP analog, ATPγS. ATPγS is not hydrolyzed by HP0525 and is an excellent inhibitor of its ATPase activity (results not shown). The ATPγS-bound structure was obtained by using crystals grown in ammonium sulfate conditions and soaked in a solution containing 5 mM ATPγS (see Materials and methods). The structure of HP0525 in crystals grown in ammonium sulfate conditions prior to soaking ATPγS was solved and shown to contain bound sulfate (result not shown). Subsequent determination of the ATPγS–HP0525 complex showed that the bound sulfate in the HP0525–sulfate complex locates at the position of the β-phosphate of ATPγS in the ATPγS–HP0525 complex.

At the protein level, the structures of the ATPγS–HP0525 and HP0525–sulfate complexes at 2.8 Å resolution are virtually identical to that of the ADP–HP0525 complex (r.m.s.d., 0.5 Å for 323 Cα atoms). The fact that the ATPγS–HP0525 and ADP–HP0525 complexes are similar implies that nucleotide binding and not hydrolysis is responsible for ATP-induced conformational changes. This seems to be a recurring theme across diverse families of oligomeric molecular machineries exhibiting NTPase activity, as similar observations have been made in GroEL/GroES (Ranson *et al*., 2001), F1-ATPase (Abraham *et al*., 1994), myosin (Houdusse *et al*., 2000), kinesin (Rice *et al*., 1999), HslUV protease (Wang *et al*., 2001) and p97 (Zhang *et al*., 2000). Surprisingly, however, ATPγS is present at full occupancy in only one of the two molecules of HP0525 in the asymmetric unit of the crystal (Figure 2A), in contrast to two fully occupied nucleotide-binding sites in the ADP–HP0525 complex (Yeo *et al*., 2000). Such difference does not appear to be the result of higher disorder in one of the sites as the B-factor values for side chain atoms in both sites are similar. Hence, there appears to be two types of nucleotide-binding site (A and B in Figure 2) with alternating arrangement along the hexameric assembly. While site A is fully occupied, in site B the position equivalent to that of the β ATPγS phosphate appears to be partially occupied by a sulfate ion that is contributed by the ammonium sulfate that was part of the crystallization condition (see comment above). Interestingly, sulfate binding in the HP0525–sulfate complex was noticeably weaker in site B than in site A despite the fact that the two nucleotide-binding sites exhibit similar structure order (data not shown). This feature of ATPγS binding becomes even more intriguing when one considers that the two nucleotide-binding sites in ATPγS–HP0525 are almost equally accessible to solvent, and prompts us to suggest that this observation may have mechanistic significance.

The structure of ATPγS bound to site A provides a complete view of the nucleotide-binding site (Figure 2B and C). On one side, Arg113 has undergone a dramatic conformational change to provide complementary electrostatic interactions to the negatively charged γ-phosphate, with Arg133, Thr180 and His273 contributing to the wall of the pocket. On the other side, Lys184 interacts directly with the γ-phosphate while Glu248 has rearranged to interact with Arg113 and His 273, poised for a catalytic role. From our studies of ADP–HP0525, which did not contain magnesium, we had proposed that the conserved Glu248 will likely coordinate to the magnesium by analogy to Glu144 of the prototypical ATPase, RecA (Story and Steitz, 1992), and that, by analogy to Glu96 in RecA, the conserved Glu209 is responsible for the activation of the attacking water during the hydrolysis of ATP (Yeo *et al*., 2000). The structure of ATPγS–HP0525 reveals that neither Glu209 nor Glu248 are within the coordination sphere of the magnesium. Instead, Glu248 is a more suitable candidate to serve as a water activator (Figure 2C). Glu209 makes a strong hydrogen bond to the water ligating to the magnesium and may play a role in stabilizing the hydrolytic transition state. Side chain conformations in site B are different and virtually identical to sites A and B in the sulfate-bound state of the enzyme (results not shown). Thus, as sulfate bears no relevance to

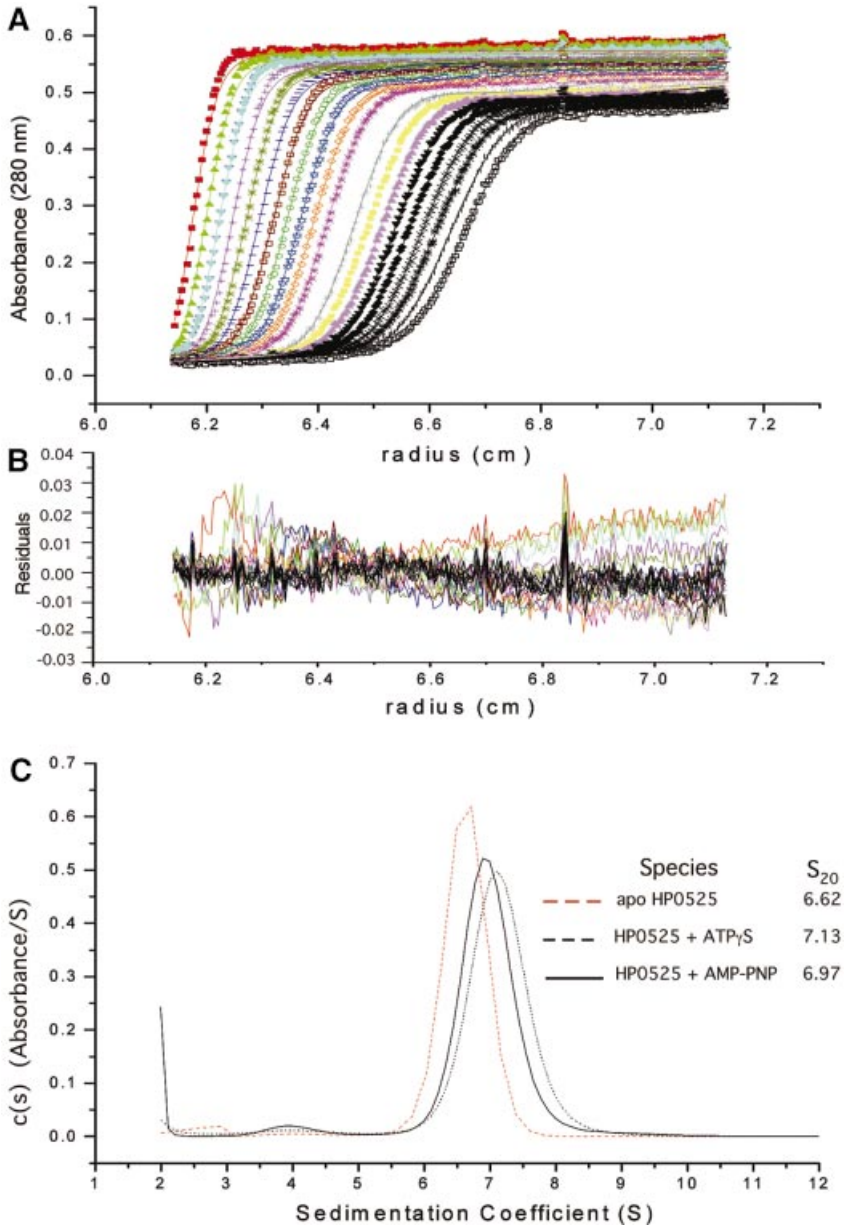

Fig. 3. Sedimentation coefficient distribution analysis of apo-, ATPγS-bound and AMP-PNP-bound HP0525. (**A**) Sedimentation velocity data of 5 μM HP0525 centrifuged at 40 000 r.p.m. Lines represent linear fits of the continuous c(s) conformational change model when constraining the molecular mass to 225 kDa, as a model for the sedimentation coefficient distribution of hexameric HP0525. Different colors are used to distinguish between successive data collection times. (**B**) Residuals from the linear fits described in (A). (**C**) Sedimentation coefficient distributions c(s) from the conformational change model.

the function of VirB11 ATPases, we believe that side chain conformations in site B do not reflect a functionally relevant state but rather a sulfate-bound state.

Nucleotide-dependent conformational changes in solution

The remarkable structural differences between apo-HP0525 and the nucleotide-bound forms of the enzyme prompted us to investigate further whether such large conformational changes could take place in solution. Previously, TrbB, a VirB11 ATPase involved in conjugative transfer of plasmid RP4, was shown to undergo sufficiently large conformational changes upon ATP binding that they can be detected using glycerol gradient centrifugation (Krause *et al.*, 2000a). However, no such changes were detected for HP0525 using this method. To investigate whether HP0525 undergoes conformational changes in solution, we used sedimentation velocity, a method more sensitive to macromolecular shape changes. We first performed sedimentation equilibrium experiments to ascertain that hexamer formation is not affected by the solution conditions employed and that it is not nucleotide dependent. Indeed, experiments performed at several protein concentrations in the range 0.11–2.22 μM and different rotor speeds in the presence and absence of ATPγS revealed a single identical species corresponding to a hexamer of HP0525. In contrast, sedimentation velocity experiments gave clear differences between

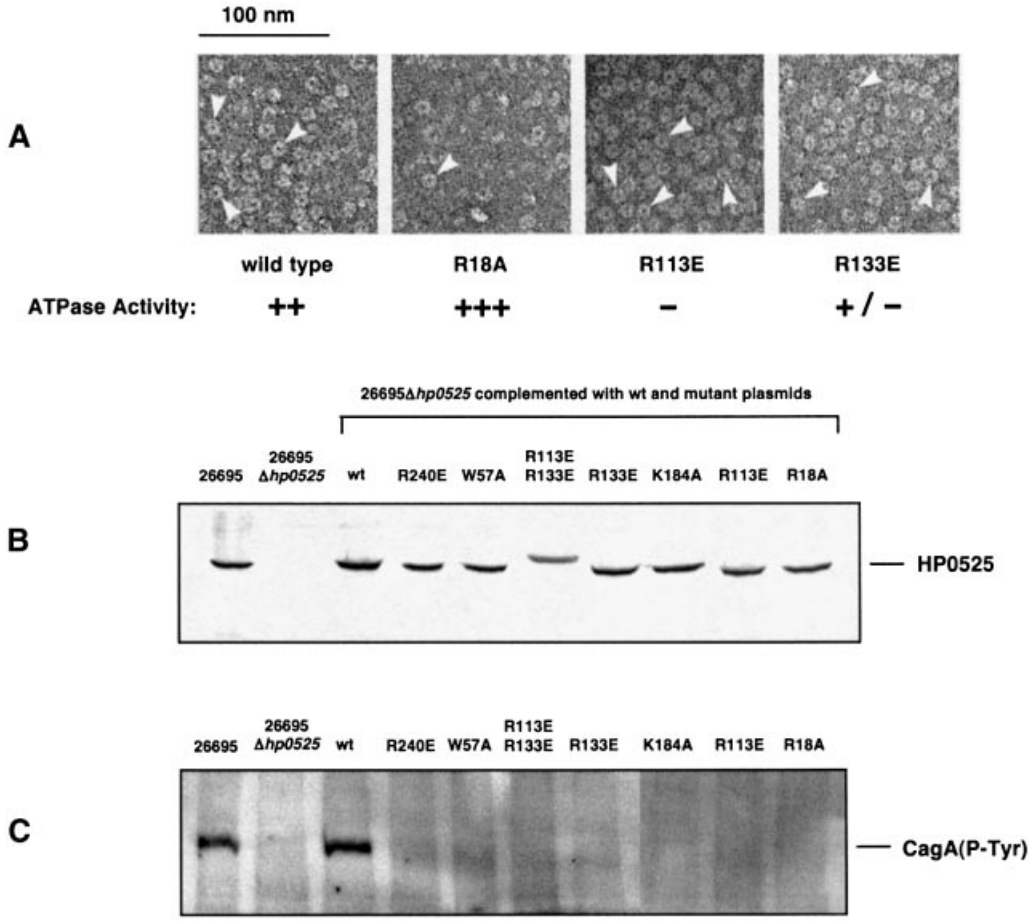

Fig. 4. Biochemical properties of HP0525 mutant proteins in *H.pylori* and test of their function in a CagA translocation assay. (**A**) Electron micrographs of negatively stained HP0525 proteins. Samples were treated as described in Krause *et al*. (2000b). Hexameric particles are indicated by white arrowheads. (**B**) Stable production of HP0525 mutant proteins after complementation of the 26695Δ*hp0525* mutant strain with the mutant genes. (**C**) HP0525-dependent transport of CagA into gastric epithelial cells.

unbound and nucleotide-bound HP0525 (differences between the two nucleotide-bound states are small and may not be significant). Binding of either ATPγS or 5′-adenyl-imido-triphosphate (AMP-PNP) causes a 5–7% increase in the sedimentation coefficient (Figure 3) indicating that HP0525 adopts a more compact structure in the presence of nucleotide, and that the conformational changes needed to elicit such a transformation are not dramatic enough to drastically change the hydrodynamic radius of the protein. Indeed, our structural studies show that the nucleotide-bound and free forms of HP0525 have similar overall dimensions with variability only between individual subunits in apo-HP0525 (Figure 1).

Mechanistic and functional insights from mutagenesis and in vivo assays

In an attempt to further understand the structural determinants dictating the formation of functional HP0525, we used a structure-based approach to generate mutants that probe three types of interaction. In the first instance, Arg18Ala-HP0525 and Trp57Ala-HP0525 were created to test oligomerization via NTD–NTD (Arg18) and NTD–CTD interactions (Trp57), respectively. Then, a series of mutations was constructed targeting a cluster of basic residues (Arg113, Arg133, Lys184 and Arg240) spanning the NTD–CTD interface and being near or part of the nucleotide-binding site. With the exception of Lys184, which was mutated to alanine (Lys184Ala), the remaining three basic residues were mutated to glutamic acid (Arg113Glu, Arg133Glu, Arg240Glu, plus the double mutant Arg113Glu/Arg133Glu). The underlying hypothesis here was that the bound nucleotide appears to neutralize otherwise repelling charges at the NTD–CTD interface (Yeo *et al*., 2000; this work). Reversing the charges of these arginines by substituting with glutamates would likely allow for favorable ionic interactions with the opposite arginines at the interface, thereby locking the HP0525 hexamer in the conformation observed in the nucleotide-bound forms.

Although all seven mutations yielded proteins that overexpressed well, only three of them (Arg18Ala, Arg113Glu and Arg133Glu) produced soluble proteins, which were further characterized biochemically. A comparison of the ability of these three mutants to form hexameric particles in the presence or absence of Mg^{2+}-ATP shows that the active-site mutants, Arg113Glu and Arg133Glu, are indistinguishable from wild type, while Arg18Ala exhibits a dramatic decrease in hexameric

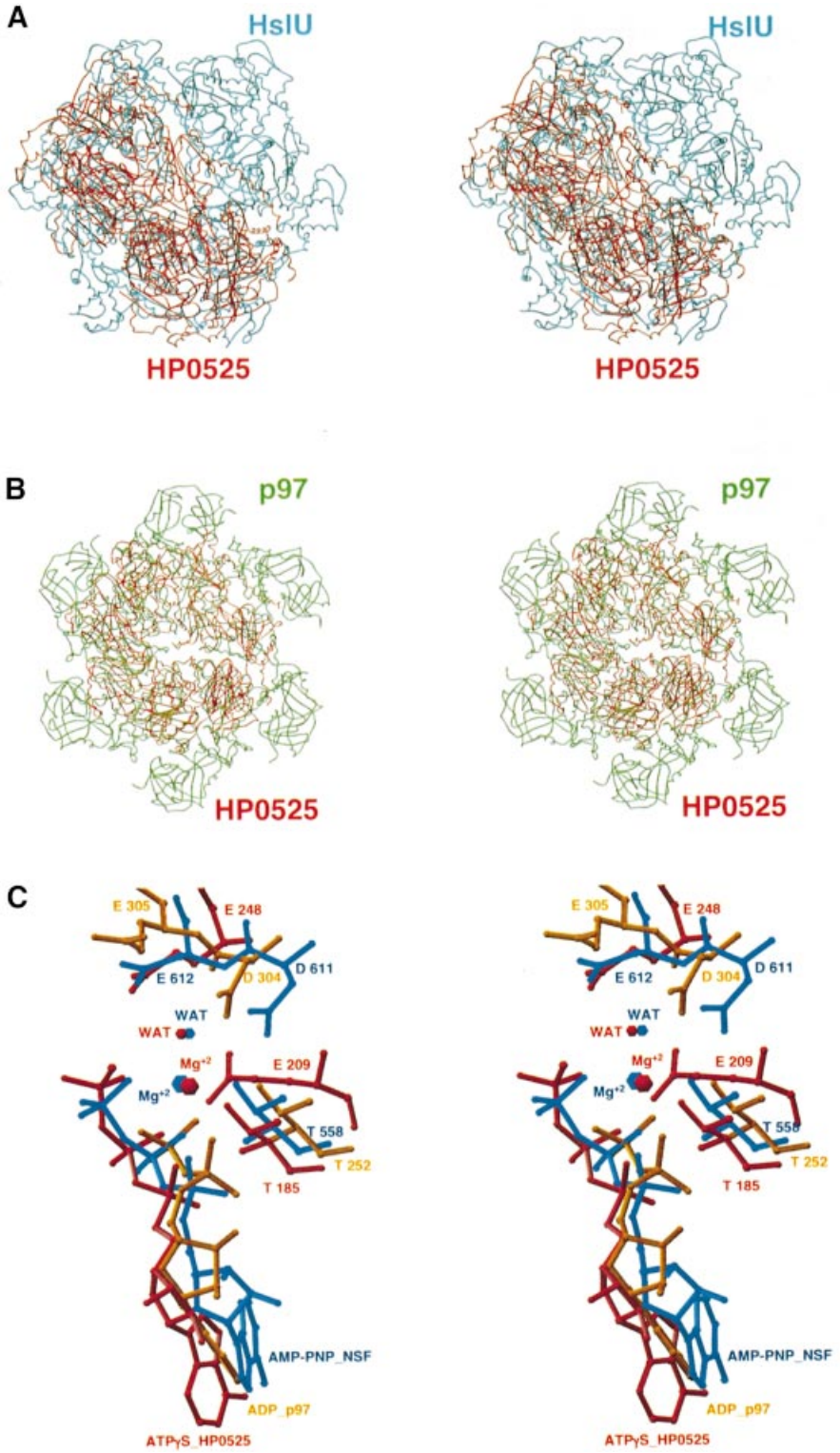

Fig. 5. Similarity of HP0525 to p97 (Carson, 1997). (**A**) Stereo diagram of a structural comparison between ADP–HP0525 (red) and ADP-bound HslU (cyan, PDB code: 1G41). The superposition is with respect to P-loop residues for one equivalent subunit from each hexamer. This figure illustrates the lack of similarity between the hexameric assembly of HP0525 and that of HslU (shown here), RecA, T7 gene 4 helicase and TrwB. (**B**) Stereo diagram of a structural comparison between ADP–HP0525 (red) and ADP-bound p97 (green, PDB code: 1E32), superimposed as in (A). p97 (shown here) and NSF are the only hexameric ATPases that have a hexameric assembly similar to HP0525. (**C**) Stereo diagram showing the structural mimicry of the DExx box motif by VirB11 ATPases, in comparison with p97 and NSF. The nucleotides and the residues of the DExx boxes are shown in ball-and-stick representation color-coded blue for the AMP-PNP –bound NSF, orange for the ADP-bound p97 and red for the ATPγS-bound HP0525.

particles and a considerable amount of disassembled oligomers (Figure 4A). The behavior of Arg18Ala with respect to hexamerization becomes particularly interesting in light of its increased ATPase activity (Figure 4A), as it appears to implicate helix αA and the NTDs in a negative cooperativity mechanism for nucleotide

binding/hydrolysis, which, in turn, may depend on either hexamer formation or perhaps on ATP-induced conformational changes in the NTDs.

In contrast to Arg18Ala, Arg113Glu and Arg133Glu exhibit a dramatic decrease in ATPase activity with Arg113Glu being completely inactive and Arg133Glu exhibiting significant activity only when assayed at a high protein concentration: such properties are consistent with their participation at the nucleotide-binding site. The more pronounced effect of the Arg113Glu is born out by our structural analysis of the ATPγS–HP0525 complex in which Arg113 appears to have a double role: to provide complementary electrostatic interaction with the ATP γ-phosphate and to interact with the catalytic Glu248 residue (Figure 2C).

To investigate the functional importance of the HP0525 site-specific mutant proteins *in vivo*, we asked whether the various HP0525 mutant proteins would be able to restore the function of the VirB11 traffic ATPase in a Δ*hp0525* background, which is to energize the *H.pylori* type IV secretion system for the translocation of the CagA protein. In infection experiments employing the mutant *H.pylori* strains only the wild-type HP0525 protein and none of the mutant proteins was able to restore the translocation and the tyrosine phosphorylation of CagA into AGS human gastric epithelial cells (Figure 4B and C). The inability of the hexamerization-impaired but ATPase-enhanced Arg18Ala protein to restore biological function, establishes that in addition to intact ATPase activity, the integrity of the HP0525 hexamer is also a key requirement for the function of VirB11 ATPases.

Role of VirB11 ATPases in bacterial type IV secretion

To gain further insights into the function and mode of action of VirB11 ATPases, we carried out structural comparisons of HP0525 with diverse hexameric ATPases such as RecA (Story and Steitz, 1992), T7 gene 4 helicase (Sawaya *et al*., 1999; Singleton *et al*., 2000), TrwB (Gomis-Rüth *et al*., 2001, 2002), HslU (Wang *et al*., 2001) and p97 AAA ATPase (Zhang *et al*., 2000). While these proteins do not share appreciable sequence similarity outside their nucleotide-binding regions, they all assemble as ring structures with similar dimensions (~110 Å in diameter and ~70 Å in height). However, when overlaid with respect to single equivalent subunits to reveal commonalities in domain and ring organization that might provide evolutionary or functional relationships, most hexameric ring structures are very different from that of HP0525, with the exception of the p97 AAA ATPase (Figure 5A and B). Like the related *N*-ethylmaleimide-sensitive fusion protein (NSF), p97 plays a central role in organelle assembly and membrane fusion processes in the endoplasmic reticulum and the Golgi apparatus (Patel and Latterich, 1998). It has a three-domain structure consisting of a flexible N-terminal domain that undergoes nucleotide-dependent conformational changes, and two C-terminal domains, D1 and D2, with folds very similar to that of the C-terminal domain of HP0525 but with only D1 supporting ATPase activity (Zhang *et al*., 2000; Rouiller *et al*., 2000).

Although HP0525 cannot readily be classified as an AAA protein due to the absence of adequate sequence similarity in the fingerprint sequences for AAA proteins, it bares remarkable structural similarities to p97. Their overall shapes are very similar (i.e. dome-like), and as in HP0525, the nucleotide-binding site is shared between the NTDs and the CTDs. Furthermore, p97 has been shown to undergo nucleotide-dependent conformational changes that affect only the NTDs while the dome-shaped hexameric structure formed by the CTDs remains intact (Rouiller *et al*., 2000). AAA proteins are characterized by a DExx box (or Walker B motif) that participates in the nucleotide-binding site and plays a catalytic role. While such a motif is absent in VirB11 ATPases, the strictly conserved Glu209 and Glu248 in HP0525 appear to mimic the role of the DExx motif by occupying structurally equivalent positions at the nucleotide-binding site (Figure 5C).

The involvement of VirB11 ATPases in type IV secretion may well be analogous to that of p97 and NSF in homotypic membrane fusion and organelle biogenesis, in that they could serve as mechanical transducers providing the necessary mechanical force for the recruitment/assembly/disassembly of type IV secretion protein components, making them available for insertion into the nascent secretion apparatus and/or to facilitate substrate translocation across the inner membrane. VirB11 ATPases could carry out such activities being associated with the bacterial inner membrane or in conjunction with partner molecules. Indeed, a yeast two-hybrid analysis designed to elucidate candidate interactions between proteins in *H.pylori* has proposed a number of such partners, most of which are yet to be annotated to biological pathways (Rain *et al*., 2001). Furthermore, a recent high-resolution yeast two-hybrid study in *Agrobacterium tumefaciens* identified several protein partners for VirB11 from within the group of Vir-encoded proteins of the type IV secretion system (Ward *et al*., 2002). Of special interest is the identification of the NTDs of VirB11, not the CTDs, as the mediators of these interactions (Ward *et al*., 2002), suggesting that the NTDs are the most likely effectors of VirB11 ATPase activities. The observed conformational variability and flexibility in the NTDs could well serve such activities by facilitating insertion into target complexes or partner molecules. Subsequent nucleotide binding could lock the protein into a rigid conformation, which following hydrolysis and ADP release, could generate the necessary mechanical force to pry open a macromolecular interaction. The structural similarity between ADP–HP0525 and ATPγS–HP0525 suggests that nucleotide binding is the critical step for biological activity, and that ATP hydrolysis may serve to accelerate nucleotide release to regenerate nucleotide-free protein for another cycle of activity.

Based on the insights we have gained here, we envision the mode of action as a four-step process combining sequential binding of nucleotides until all available sites are filled followed by nucleotide release to return to apo-HP0525 (Figure 6). Two lines of evidence point to such a mechanism: (i) the structure of the ATPγS–HP0525 complex exhibits differential occupancy of nucleotide despite equal accessibility to solvent, and (ii) apo-HP0525 displays modular behavior between opposing subunits in the hexameric ring. Such nucleotide-binding patterns are reminiscent of those observed in T7 gene 4 helicase

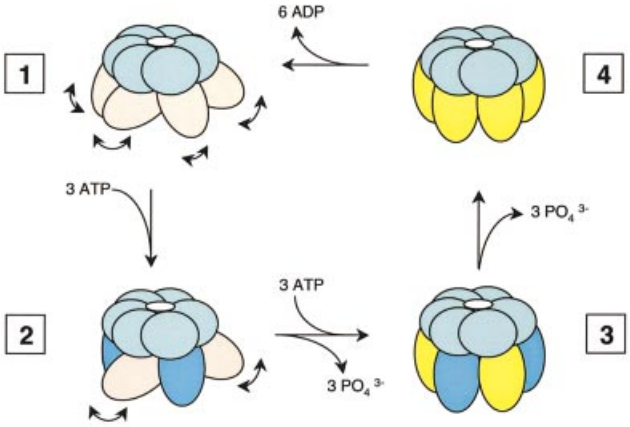

Fig. 6. Model for the mode of action of VirB11 ATPases. The N-terminal and C-terminal domains are represented in pink and light blue, respectively. NTDs locked in a rigid conformation by the binding of ATP and ADP are shown in cyan and yellow, respectively.

(Singleton *et al*., 2000) and in the HslU AAA protein (Wang *et al*., 2001). The proposed mechanism is described in Figure 6 and is as follows. Step 1: the nucleotide-free form exists as an asymmetric hexamer exhibiting mobility of the NTD (pink) while the CTDs (light blue) are responsible for maintaining a pseudo-hexameric scaffold; VirB11 ATPases in this molecular state likely use their flexibility to bind effectively to target macromolecular complexes. Step 2: the binding of three ATP molecules locks three subunits into a rigid conformation. Step 3: hydrolysis of the three ATPs to ADP with concomitant binding of ATP to the remaining three nucleotide-free subunits results in a perfectly hexameric rigid form. Step 4: the structure retains its symmetry and rigidity until all ATP molecules are hydrolyzed, at which point HP0525 can return to its nucleotide-free form.

While a more systematic mutagenesis study coupled with kinetics will be necessary to fully dissect the structural determinants of the function and mode of action of VirB11 ATPases (notably to establish the proposed alternating ATP-binding model), the findings we report here provide concrete support for the dynamic nature of VirB11 ATPases and for their candidacy as drug targets against pathogenic bacteria, as single amino acid substitutions of just one protein member of the *H.pylori* type IV secretion are enough to abrogate secretion of the pathogenic substrate. Our analysis also suggests that a drug design effort could follow two directions in parallel, one targeting the ATPase activity and one disrupting hexamer formation.

Materials and methods

Crystallization of apo-HP0525 and ATPγS–HP0525, and data collection

Purified HP0525 (Yeo *et al*., 2000) was crystallized under two different conditions. Form-A crystals appeared in 48 h as hexagonal plates using a reservoir solution containing 2 M ammonium sulfate, 2% PEG 400 and 100 mM Tris–HCl pH 7.8. Form-B crystals appeared in 1 week, exhibiting a cone-shaped morphology, and grew from a reservoir solution containing 18% polyethylene glycol monomethyl ether 2000 (PEG-MME-2000), 0.1 M NaCl and 200 mM Tris–HCl pH 6.9. Form-A crystals were cryo-cooled to liquid nitrogen temperature after progressive (over 20 min) transfer to a stabilizing solution containing 2.4 M ammonium sulfate, 2% PEG 400, 100 mM Tris–HCl pH 7.8 and increasing glycerol concentrations [25% (v/v) final]. The ATPγS–HP0525 complex was prepared from form-A crystals (termed ATPγS–HP0525 crystals) due to their stability in cryo-protecting solution containing ATPγS/$MgCl_2$. Specifically, form-A crystals were incubated in the final cryo-solution supplemented with 5 mM ATPγS/$MgCl_2$ for 3 days and were subsequently cryo-cooled for data collection. Form-B crystals were cryo-cooled to liquid nitrogen temperature after a brief incubation in 20% PEG-MME-2000, 0.1 M NaCl, 200 mM Tris–HCl pH 6.9 and 25% (v/v) glycerol.

Form-A and ATPγS–HP0525 crystals belong to space group $P6_322$ with two molecules in the asymmetric unit and cell dimensions $a = b =$ 111.3 Å, c = 230.2 Å and $a = b$ = 110.8 Å, c = 230.9 Å, respectively. On the other hand, form-B crystals belong to space group $P3_1$ with cell dimensions $a = b$ = 104.5 Å, c = 168.7 Å and six molecules in the asymmetric unit. Data were collected from form-A and ATPγS–HP0525 crystals to 2.8 Å resolution, and from form-B crystals to 3.0 Å resolution at beamline 19BM (Structural Biology Center, Advanced Photon Source) (Table I). Data were processed with DENZO and SCALEPACK (Otwinowski and Minor, 1997).

Structure determination and refinement

The structure of apo-HP0525 was determined from form-B crystals at 3.0 Å resolution by multi-wavelength anomalous diffraction (MAD) using the program SOLVE (Terwilliger and Berendzen, 1999; Terwilliger, 2000) (Table I). The experimental electron density revealed that each of the six molecules exhibited rigid-body NTD domain shifts about the linker region between the NTDs and CTDs (residues 133–142). Individual domains were built using the program O (Jones *et al*., 1991) and the structure was refined to 3.0 Å resolution by torsion-angle simulated-annealing and conjugate-gradient minimization using CNS (Brünger *et al*., 1998) (Table I). Initially, heavy NCS restraints (300 kcal/mol/Å^2) were applied uniformly to main chain atoms in all six molecules, but were adjusted during the course of refinement to values (100 and 50 kcal/mol/Å^2 for NTD and CTD, respectively) that optimized the R_{free} value. The model includes residues 6–328 for molecule A, residues 22–328 for molecule B, residues 28–76 and 101–330 for molecule C, residues 10–329 for molecule D, residue 24–328 for molecule E and residue 24–328 for molecule F. All ϕ/ψ angles lie in the allowed regions of the Ramachandran plot with 85% in the most favored regions.

The structures of form-A and ATPγS–HP0525 crystals were determined in parallel. Because the crystals were nearly isomorphous to those of ADP–HP0525, *de novo* phasing was not necessary. Thus, the refined model of ADP–HP0525 (PDB accession code 1g6o) without water and ADP molecules was used in rigid-body refinement followed by torsion-angle simulated annealing and conjugate-gradient minimization using CNS (Brünger *et al*., 1998). NCS restraints were applied to main chain atoms and were optimized (200 and 100 kcal/mol/Å^2 for form-A and ATPγS–HP0525 crystals, respectively). After initial refinement, $2F_o–F_c$ and $F_o–F_c$ difference Fourier electron density maps contoured at 1σ and 3σ, respectively, were used to assess the structures. Electron density maps for form-A crystals unambiguously showed the presence of sulfate ions (most likely contributed by the crystallization conditions) in both molecules in the asymmetric unit, at positions corresponding to the β-phosphate of the nucleotide. Sulfate ions were included in the model only in the last two rounds of refinement to minimize model bias. The final model of the HP0525–sulfate complex (Table I) exhibits good stereochemistry with 85% of all ϕ/ψ angles in the most favored regions of the Ramachandran plot (none in disallowed regions). In the case of ATPγS–HP0525 crystals, we observed ATPγS and Mg^{2+} in molecule A at high occupancy but only partial binding in molecule B. Interestingly, the electron density corresponding to the β-phosphate of the nucleotide at this position was markedly higher and therefore not consistent with that for the rest of the nucleotide, suggesting that sulfate (part of the crystallization condition) partially occupied the site. While ATPγS and Mg^{2+} were readily modeled in molecule A, test refinements consisting of 20 cycles of conjugate-gradient minimization followed by 20 cycles of B-factor refinements with various complementary occupancy combinations of ATPγS and sulfate were needed to estimate the relative occupancy of these two ligands in molecule B. A model with occupancies of 0.5 for each ATPγS and sulfate yielded B-factors for ATPγS that were consistent with those of the nucleotide in molecule A, and produced the lowest R_{free} value and no residual electron density in $F_o–F_c$ difference fourier maps, indicating that the site was adequately modeled. The final model has good stereochemistry with 86% of all ϕ/ψ angles in the most favored regions of the Ramachandran plot (none in disallowed regions).

The coordinates of apo-HP0525 (entry code 1NLZ), ATPγS–HP0525 (entry code 1NLY) and HP0525–sulfate (entry code 1OPX) have been deposited in the Protein Data Bank (www.rcsb.org).

Analytical ultracentrifugation

Sedimentation experiments were conducted using a Beckman XL-A Optima analytical ultracentrifuge equipped with absorbance optics and a Ti-60a titanium rotor. Sedimentation equilibrium studies were carried out at 10 000, 14 000 and 20 000 r.p.m., at 25°C. Six-channel, charcoal-filled epon centerpieces with quartz windows were filled with 120 µl of sample (in 20 mM HEPES, 100 mM NaCl, 1 mM DTT, 10% glycerol pH 7.0) at concentrations between 111 nM and 2.22 µM, in the absence and presence of nucleotide at 100-fold excess over protein concentration. Absorbance profiles were acquired at a wavelength of 230 or 280 nm, chosen according to the protein concentration. Sedimentation equilibrium distributions were fit to a single species using global non-linear least squares techniques (program NONLIN; Johnson *et al*., 1981). When the molar mass is treated as the unknown parameter in the global analysis, an average molecular weight of 274 694 Da is obtained (compared with the expected molecular weight of 225 432 Da for hexameric HP0525). Attempts to fit the data to a self-association model failed to yield better results. From the sedimentation equilibrium data alone, it cannot be ruled out that there might be a significant population of several different oligomeric species. However, the boundary spreading in further sedimentation velocity experiments is consistent with that of a single hexameric species.

Sedimentation velocity experiments were carried out at 40 000 r.p.m. at 25°C in double sector epon centerpieces. Data were collected at 280 nm and at a radial increment of 0.01 cm with four averages in a continuous scan mode. Data analysis was carried out using SEDFIT (Schuck *et al*., 2002), which employs the continuous c(s) conformational change model based on the Lamm equation, to determine the sedimentation coefficient distribution.

Mutagenesis and preparation of mutant proteins

HP0525 mutants R18A, W57A, R113E, R133E, K184A, R240E were generated using the QuickChange site-directed mutagenesis kit (Stratagene) using plasmid pWP4760 as the template (Krause *et al*., 2000b), and were verified by sequencing. The double mutant R113E/R133E was constructed using plasmid pWP4760/R133E as the template.

Cultures of SCS1 cells containing the mutated plasmids were grown at 37°C to an OD_{600} of ~0.5. Protein expression was induced by 1 mM IPTG for 4 h at 37°C. Proteins R18A, R113E, R133E and R113+133E are soluble, but not the mutants proteins W57A and K184A. Protein purification was carried out as described previously (Krause *et al*., 2000a) with the following modifications: in the first step, Q-Sepharose was used instead of HiTrapQ, and in the last step, Heparin HiTrap was used instead of a Superose-12 gel filtration. Proteins R18A, R113E and R133E could be purified using this purification protocol, whereas protein R113+133E could not be separated from the bulk of proteins despite the inclusion of additional chromatographic steps.

ATPase activity

Two ATPase assays were performed. In a first assay, 15 or 50 pmol HP0525 were incubated for 30 min at 30°C in 20 mM Tris–HCl pH 7.6, 50 mM NaCl, 5 mM $MgCl_2$, 1 mM DTT, 50 µg/ml BSA supplemented by 200 µM ATP and 100 nCi [γ-^{32}P]ATP in a total volume of 20 µl. The reaction was stopped with 25 mM EDTA. A 2 µl aliquot of the reaction mixture was analyzed by thin-layer chromatography and reaction products were quantified using a phosphorimager. In a second assay, the P_iPer phosphate assay kit (Molecular Probes) monitoring inorganic phosphate release was used according to the manufacturer's instructions.

Construction of plasmids for complementation assays and transformation of H.pylori

Mutant genes were amplified by PCR from plasmids pWP4760R240E, pWP4760W57A, pWP4760R113E+R133E, pWP4760R133E, pWP4760-K184A, pWP4760R113E and pWP4760R18A using primers WS156 (5′-ACCGCTCGAGCTTTAAGAAGGAGATATACATATGACTGAA-GACAGATTGA-3′) (*Xho*I-T7-geneX-SD-*Nde*I-*hp0525*) and RB23 (5′-CGGGATCCTACCTGTGTTTGATATAAAATTCA-3′) (*Bam*HI-*hp0525*, 3′end). The PCR products were cloned as *Bam*HI–*Xho*I fragments into pJP99 (Püls *et al*., 2002). The pJP99 suicide plasmids containing the mutant *hp0525* genes were introduced into *H.pylori* 26695Δ*hp0525* by natural transformation as described previously (Haas *et al*., 1993).

SDS–PAGE, immunoblotting of CagA and detection of tyrosine-phosphorylated proteins

Lysates of bacteria or infected cells were subjected to SDS–PAGE and were blotted onto a PVDF membrane. For detection of CagA, the filters were blocked with 3% BSA in 50 mM Tris–HCl pH 7.5, 150 mM NaCl, and incubated with the antiserum AK257 (an anti-αCagA antibody). Alkaline phosphatase-coupled protein A was used to visualize the antibody bound by decomposition of nitro-blue tetrazolium. For detection of tyrosine-phosphorylated proteins the blot was blocked overnight in 50 mM Tris pH 7.4, 200 mM NaCl, 0.1% Tween-20, 5% milk powder. The phosphotyrosine-specific monoclonal antibody PY99 (Santa Cruz Biotechnology, Inc.) was applied for detection of phosphorylated CagA using the Renaissance detection system (NEN).

AGS infection and tyrosine phosphorylation assay

These experiments were performed as in Odenbreit *et al*. (2000). In brief, AGS cells were grown in six-well plates (9.5 cm^2) and infected with *H.pylori* at a m.o.i. of 100. Non-adherent bacteria were removed by washing in PBS (five times). Cells were suspended in 1 ml ice-cold PBS* (PBS, 1 mM EDTA, 1 mM *o*-vanadate, 1 mM phenylmethane sulfonyl fluoride, 1 µM leupeptin, 1 µM pepstatin) with a cell scraper, collected by centrifugation and resuspended in 30 µl PBS*. The samples were then analyzed by SDS–PAGE .

Acknowledgements

We thank the staff of beamline 19BM of the Structural Biology Center at APS (Argonne National Laboratory) for help during data collection. This work was supported by NIH grant AI49950 and Wellcome Trust grant 065932 to G.W., DFG grant GK303/2 to R.H. and the European Commission grant QLK2-CT-2000-01624 to E.L.

References

Abraham,J.P., Leslie,A.G.W., Lutter,R. and Walker,J.E. (1994) Structure at 2.8 Å resolution of F1-ATPase from bovine heart mitochondria. *Nature*, **370**, 621–628.

Asahi,M., Azuma,T., Ito,S., Ito,Y., Suto,H., Nagai,Y., Tsubokawa,M., Tohyama,Y., Maeda,S., Omata,M., Suzuki,T. and Sasakawa,C. (2000) *Helicobacter pylori* CagA protein can be tyrosine phosphorylated in gastric epithelial cells. *J. Exp. Med.*, **191**, 593–602.

Backert,S., Ziska,E., Brinkmann,V.Z.-A.U., Fauconnier,A., Jungblut,P.R., Naumann,M. and Meyer,T.F. (2000) Translocation of the *Helicobacter pylori* CagA protein in gastric epithelial cells by a type IV secretion apparatus. *Cell. Microbiol.*, **2**, 155–164.

Brünger,A.T. *et al.* (1998) Crystallography and NMR system: a new software suite for macromolecular structure determination. *Acta Crystallogr. D*, **54**, 905–921.

Carson,M. (1997) Ribbons. *Methods Enzymol.*, **277**, 493–505.

Christie,P.J. and Vogel,J.P. (2000) Bacterial type IV secretion: conjugation systems adapted to deliver effector molecules to host cells. *Trends Microbiol.*, **8**, 354–360.

Finlay,B.B. and Falkow,S. (1997) Common themes in microbial pathogenicity revisited. *Microbiol. Mol. Biol. Rev.*, **61**, 136–169.

Gomis-Rüth,F.X., Moncalián,G., Pérez-Luque,R., González,A., Cabezón,E., de la Cruz,F. and Coll,M. (2001) The bacterial conjugation protein TrwB resembles ring helicases and F1-ATPase. *Nature*, **409**, 637–641.

Gomis-Rüth,F.X., Moncalián,G., de la Cruz,F. and Coll,M. (2002) Conjugative plasmid protein TrwB, an integral membrane type IV secretion system coupling protein. *J. Biol. Chem.*, **277**, 7556–7566.

Graham,D.Y. (2000) *Helicobacter pylori* infection is the primary cause of gastric cancer. *J. Gastroenterol.*, **35**, 90–97.

Haas,R., Meyer,T.F. and van Putten,J.P.M. (1993) A flagellated mutant of *Helicobacter pylori* generated by genetic transformation of naturally competent strains using transposon shuttle mutagenesis. *Mol. Microbiol.*, **8**, 753–760.

Houdusse,A., Szent-Gyorgyi,A.G. and Cohen,C. (2000) Three conformational states of scallop myosin S1. *Proc. Natl Acad. Sci. USA*, **97**, 11238–11243.

Johnson,M.L., Correia,J.J., Yphantis,D.A. and Halvorson,H.R (1981) Analysis of data from the analytical ultracentrifuge by nonlinear least-squares techniques. *Biophys. J.*, **36**, 575–588.

Jones,T.A., Zou,J.Y., Cowan,S.W. and Kjeldgaard,M. (1991) Improved

methods for building protein models in electron density maps and the location of errors in these models. *Acta Crystallogr. A*, **47**, 110–119.
Krause,S., Barcena,M., Pansegrau,W., Lurz,R., Carazo,J.M. and Lanka,E. (2000a) Sequence-related protein export NTPases encoded by the conjugative transfer region of RP4 and by the cag pathogenicity island of *Helicobacter pylori* share similar hexameric ring structures. *Proc. Natl Acad. Sci. USA*, **97**, 3067–3072.
Krause,S., Pansegrau,W., Lurz,R., de la Cruz,F. and Lanka,E. (2000b) Enzymology of type IV macromolecule secretion systems: the conjugative transfer regions of plasmids RP4 and R388 and the cag pathogenicity island of *Helicobacter pylori* encode structurally and functionally related nucleoside triphosphate hydrolases. *J. Bacteriol*., **182**, 2761–2770.
Lenzen,C.U., Steinmann,D., Whiteheart,S. and Weis, W.I. (1998) Crystal structure of the hexamerization domain of *N*-ethylmaleimide-sensitive fusion protein. *Cell*, **94**, 525–536.
Machón,C., Rivas,S., Albert,A., Goñi,F.M. and de la Cruz,F. (2002) TrwD, the hexamerix traffic ATPase encoded by plasmid R388, induces membrane destabilization and hemifusion of lipid vesicles. *J. Bacteriol*., **184**, 1661–1668.
Odenbreit,S., Püls,J., Sedlmaier,B., Gerland,E., Fischer,W. and Haas,R. (2000). Translocation of *Helicobacter pylori* CagA into gastric epithelial cells by type IV secretion. *Science*, **287**, 1497–1500.
Otwinowski,O. and Minor,W. (1997) Processing of X-ray diffraction data collected in oscillation mode. *Methods Enzymol.*, **276**, 307–326.
Patel,S. and Latterich,M. (1998) The AAA team: related ATPases with diverse functions. *Trends Cell Biol.*, **8**, 65–71.
Possot,O. and Pugsley,A.P. (1994) Molecular characterization of PulE, a protein required for pullulanase secretion. *Mol. Microbiol.*, **12**, 287–299.
Püls,J., Fischer,W. and Haas,R. (2002) Activation of *Helicobacter pylori* CagA by tyrosine phosphorylation is essential for dephosphorylation of host cell proteins in gastric epithelial cells. *Mol. Microbiol.*, **43**, 961–969.
Rain,J.C. *et al.* (2001) The protein–protein interaction map of *Helicobacter pylori*. *Nature*, **409**, 211–215.
Ranson,N.A., Farr,G.W., Roseman,A.M., Gowen,B., Fenton,W.A., Howich,A.L. and Saibil,H.R. (2001) ATP-bound states of GroEL captured by cryo-electron microscopy. *Cell*, **107**, 869–879.
Rashkova,S., Spudich,G.M. and Christie,P.J. (1997) Characterization of membrane and protein interaction determinants of the *Agrobacterium tumefaciens* VirB11 ATPase. *J. Bacteriol*., **179**, 583–591.
Rice,S. *et al.* (1999) A structural change in the kinesin motor protein that drives motility. *Nature*, **402**, 778–784.
Rouiller,I., Butel,V.M., Latterich,M., Milligan,R.A. and Wilson-Kubalek,E.M. (2000) A major conformational change in p97 AAA ATPase upon ATP binding. *Mol. Cell*, **6**, 1485–1490.
Sawaya,M.R., Guo,S., Tabor,S., Richardson,C.C. and Ellenberger,T. (1999) Crystal structure of the helicase domain from the replicative helicase-primase of bacteriophage T7. *Cell*, **99**, 167–177.
Schuck,P., Perugini,M.A., Gonzales,N.R., Howlett,G.J. and Schubert,D. (2002) Size-distribution analysis of proteins by analytical ultracentrifugation: strategies and application to model systems. *Biophys. J.*, **82**, 1096–1111.
Segal,E.D., Cha,J., Lo,J., Falkow,S. and Tompkins,L.S. (1999) Altered states: involvement of phosphorylated CagA in the induction of host cellular growth changes by *Helicobacter pylori*. *Proc. Natl Acad. Sci. USA*, **96**, 14559–14564.
Singleton,M.R., Sawaya,M.R., Ellenberger,T. and Wigley,D.B. (2000) Crystal structure of T7 gene 4 ring helicase indicates a mechanism for sequential hydrolysis of nucleotides. *Cell*, **101**, 589–600.
Stein,M., Rappuoli,R. and Covacci,A. (2000) Tyrosine phosphorylation of the *Helicobacter pylori* CagA antigen after *cag*-driven host cell translocation. *Proc. Natl Acad. Sci. USA*, **97**, 1263–1268.
Story,R.M. and Steitz,T.A. (1992) Structure of the recA protein–ADP complex. *Nature*, **355**, 374–376.
Terwilliger,T.C. (2000) Maximum-likelihood density modification. *Acta Crystallogr. D*, **56**, 965–972.
Terwilliger,T.C. and Berendzen,J. (1999) Automated MAD and MIR structure solution. *Acta Crystallogr. D*, **55**, 849–861.
Thanassi,D.G. and Hultgren,S.J. (2000) Multiple pathways allow protein secretion across the bacterial outer membrane. *Curr. Opin. Cell Biol.*, **12**, 420–430.
Vogel,J.P., Andrews,H.L., Wong,S.K. and Isberg,R.R. (1998) Conjugative transfer by the virulence system of *Legionella pneumophila*. *Science*, **279**, 873–876.
Wang,J., Song,J.J., Seong,I.S., Franklin,M.C., Kamtekar,S., Eom,S.H. and Chung,C.H. (2001) Nucleotide-dependent conformational changes in a protease-associated ATPase HslU. *Structure*, **9**, 1107–1116.
Ward,D.V., Draper,O., Zupan,J.R. and Zambryski,P.C. (2002) Peptide linkage mapping of the *Agrobacterium tumefaciens vir*-encoded type IV secretion system reveals protein subassemblies. *Proc. Natl Acad. Sci. USA*, **99**, 11493–11500.
Wotherspoon,A.C. (1998). Gastric lymphoma of mucosa-associated lymphoid tissue and *Helicobacter pylori*. *Annu. Rev. Med.*, **49**, 289–299.
Ye,Y., Meyer,H.H. and Rapoport,T. (2001) The AAA ATPase Cdc48/p97 and its partners transport proteins from the ER into the cytosol. *Nature*, **414**, 652–656.
Yeo,H.-J., Savvides,S.N., Herr,A.B., Lanka,E. and Waksman,G. (2000) Crystal structure of the hexameric traffic ATPase of the *Helicobacter pylori* type IV secretion system. *Mol. Cell*, **6**, 1461–1471.
Zhang,X. *et al.* (2000) Structure of the AAA ATPase p97. *Mol. Cell*, **6**, 1473–1484.

Received December 3, 2002; revised February 3, 2003; accepted March 17, 2003